

This is a postprint version of the following published document:

González-Benito, J., Teno, J., González-Gaitano, G., Xu, S. & Chiang, M. (2017). PVDF/TiO₂ nanocomposites prepared by solution blow spinning: Surface properties and their relation with S. Mutans adhesion. *Polymer Testing*, vol. 58, pp. 21–30.

DOI: [10.1016/j.polymertesting.2016.12.005](https://doi.org/10.1016/j.polymertesting.2016.12.005)

© 2016 Elsevier Ltd.



This work is licensed under a [Creative Commons Attribution-NonCommercial-NoDerivatives 4.0 International License](https://creativecommons.org/licenses/by-nc-nd/4.0/).

PVDF/TiO₂ Nanocomposites Prepared by Solution Blow Spinning: Surface Properties and their Relation with *S. mutans* Adhesion

J. González-Benito^{1*}, J. Teno¹, G. González-Gaitano², S. Xu³, M. Chiang³

¹*Dept. Materials Science and Engineering, IQMAAB, Universidad Carlos III de Madrid, Madrid, SPAIN*

²*Dept. Química, Facultad de Ciencias, Universidad de Navarra, 31080, Pamplona, SPAIN.*

³*Polymers Division, National Institute of Standards and Technology, Gaithersburg, MD 20899-8544, USA*

*To whom all correspondences should be addressed

Address: Av. Universidad 30, 28911 Leganés (Madrid – Spain)

e-mail: javid@ing.uc3m.es

Abstract

Thermoplastic nanocomposite materials with potential bactericide properties were prepared and their surface properties and adhesion to *Streptococcus mutans*, *S. mutans*, were characterized. Solution blow spinning was successfully used to prepare films with a fiber-like structure on the surface of nanocomposites based on Polyvinylidene fluoride, PVDF, filled with well dispersed TiO₂ nanoparticles. PVDF/TiO₂ nanocomposites were prepared varying the nanoparticles content (0 %, 1 %, 2 %, 5 % and 10 % by weight). In order to understand the influence of the presence of TiO₂ nanoparticles and the final surface properties on the adhesion of *S. mutans* to the materials, a deep characterization was carried out focusing on the morphology, roughness, surface free energy from contact angle measurements and cell adhesion by single cell force spectroscopy. It was observed that the uniform dispersion of the nanofiller arose from nanoparticles embedded in the polymer when fibers were created during the blow spinning process. TiO₂ content influenced the topography of the films probably due to a direct effect on the solvent evaporation rate. Although this factor greatly conditioned the roughness of the samples and therefore the surface free energy, *S. mutant* adhesion on the substrates under study was concluded to be more dependent on the specific interactions with the surface polar groups of the material.

Keywords: PVDF; TiO₂; blow spinning; nanocomposites; cell adhesion.

1. Introduction

The use of plastics in the field of biomaterials is growing nowadays, for instance, in the form of prosthesis, catheters, scaffolds for tissue engineering, wound healing, etc. In these applications or devices, apart from having intrinsic good mechanical properties and avoid proliferation of harmful microorganisms, they should be able to be prepared for their final use in a straightforward way, even though with the possibility of being generated *in-situ*. In this sense, thermoplastic materials are the best choice as they can be easily prepared with different morphologies and complex forms for the required application by extrusion, molding, injection or dissolution, among other methods. In particular, nanofiber mats of thermoplastics are receiving a special attention due to their potential use as materials for drug delivery [1], wound dressings [2–4], tissue engineering [5,6], etc. Probably the most extended method to prepare this kind of mats is electrospinning, a process in which a polymer ejected solution is subjected to an electric field which deforms it to generate nanofibers [7]. However, the use of high voltages in electrically conductive targets where the fibers are deposited and the low deposition rates make necessary to look for other more versatile methods, at least for certain applications; for example, when direct dispensation of the materials is required, as in surgery or in-situ creation of wound dressings. Particularly, solution blow spinning, SBS, might be a promising method. In this method, developed by Medeiros et al. to produce micro- and nanofibers of several thermoplastics [8], the spinning system consists of concentric nozzles through which a polymer solution and a pressurized gas are simultaneously ejected. Therefore, apart from the same applications than

other methods used to prepare mats or films like electrospinning, SBS might be used in-situ in a very fast way, for instance, after surgical practices to seal bounds, cover or coat other materials, etc. Probably the greater inconvenience in SBS is to find the proper solvent or mixture of solvents: i) to create the expected morphology and, ii) without harmful properties in the case of direct use in a human body.

Therefore, the materials here considered must have good mechanical and optical properties apart from presenting the ability of being easily processed and, if possible, they should avoid proliferation of harmful microorganisms. To account for all those requirements, thermoplastic polymers filled with nanoparticles having highly specific properties such as bactericidal effect may be a good choice. Among the thermoplastic polymers to prepare the final nanocomposites with the desired properties polyvinylidene fluoride, PVDF, may be a good choice since it is very resistant to pH variations, biocompatible and has peculiar piezoelectric properties what might make it the focus of multiple applications [9]. On the other hand, TiO₂ nanoparticles can be selected as the filler because of its potentiality as biocidal material [10–15]. Although the activity of TiO₂ is simultaneously combined with the irradiation of UV light, recent studies point out that TiO₂ can also affect bacterial growth in the absence of UV light [10,11,16–18]. Besides, the nanoscopic character of the particles allows them to be added in low amount because their large surface to volume ratio implies the creation of so large interphase as to significantly change the polymer matrix properties.

In particular the system based on PVDF filled with TiO₂ particles is receiving nowadays great interest. For instance Muñoz-Bonilla et al. prepared highly efficient antibacterial nanocomposite films consisting of a commercially available poly(vinylidene difluoride) (PVDF) incorporating synthesized TiO₂ with absence of solvents [19]. On the other hand, Hamzah et al. fabricated PVDF/TiO₂ membranes with and without silane modification and their separation performance, fouling and self-cleaning property were evaluated [20]. Other work use the addition of TiO₂ to PVDF and copolymer with the final objective of changing electrical properties [21]. Among others, new possible application of those biocompatible materials may be focused to cover or coating bounds created after surgical interventions in mouth.

Although the antibacterial effect can be attributed to a direct influence of a certain material on the bacteria metabolism (biocide behavior), many times the effect is associated to an inhibition of biofilm development by poor cell adhesion to the material. To clarify this, deeper investigation about this issue should be carried out. In other words, before facing the description and explanation of biofilms development, data about interactions between a surface of a certain substrate and a specific cell should be collected and analyzed.

A systematic investigation about the effect of the surface chemistry on the bacterial adhesion has been reported [22]. In particular, a number of relevant physicochemical factors when defining the surface at the molecular level were assessed for their effect on the adhesion of *Listeria monocytogenes*, *Salmonella typhimurium*, *Staphylococcus aureus*, and *Escherichia coli*, concluding that, for a particular substrate-bacteria system, detailed studies about the surface features (morphology, roughness, surface free energy) and cell adhesion must be carried out to understand the possible antibacterial properties. Therefore, an atomic force microscope, AFM, may be an ideal tool to study the adhesion force of a single cell by obtaining force curves as a function of distance [23].

In particular, the adhesion of a cell can be measured by pull-off tests performed with the AFM by the so-called single cell force spectroscopy technique [24,25].

Streptococcus mutans are bacteria commonly found in the human oral cavity and is an important cause of teeth deterioration and oral diseases. Due to this, studies related with their proliferation on materials that could be found within the mouth should be done. Taking into account the above cited properties, if PVDF based materials are thought to be interesting to be applied in mouth in surgical interventions, as restorative material or other applications, the adhesion of *S. mutant* onto them should be studied.

In this work, solution blow spinning, SBS, has been used as a novel way of preparing nanocomposites based on PVDF filled with well dispersed TiO₂ nanoparticles with potential antibacterial activity. As a function of the nanoparticles content morphology studies based on the observation of the dispersion of the nanoparticles within the polymer have been performed, as well as an in-depth characterization of the surface of the materials (morphology, topography, wettability and surface free energy). All these data were used to explore and establish correlations with data coming from single cell force spectroscopy, carried out in two sample PVDF with and without TiO₂ nanoparticles, about the adhesion of *Streptococcus mutans* to the nanocomposites surface.

2. Experimental

2.1 Materials

As the matrix for the composites polyvinylidene fluoride, PVDF, (Sigma-Aldrich; Mn ~ 10.700; Mw ~ 27.500 and density 1.78 g·cm⁻³) was used. As the filler, titanium (IV) oxide nanopowder (mixture of rutile and anatase with 99.9% of purity), TiO₂, purchased from Sigma-Aldrich was used - mean diameter < 100 nm (BET) and < 50 nm (XRD) nm. Dimethylformamide, DMF, and acetone (HPLC grade), from Aldrich, were used as solvents for the solution blow spinning process.

2.2 Materials preparation

The PVDF/TiO₂ nanocomposites with different amounts of TiO₂ (0 %, 1 %, 2 %, 5 % and 10 % by weight) were prepared in the form of films by solution blow spinning, SBS, using a commercial airbrush and compressed air. Suspensions of TiO₂ nanoparticles in a PVDF solution of 10 % wt/v in a DMF/Acetone were prepared and then blow spun on glass substrates (Figure 1).

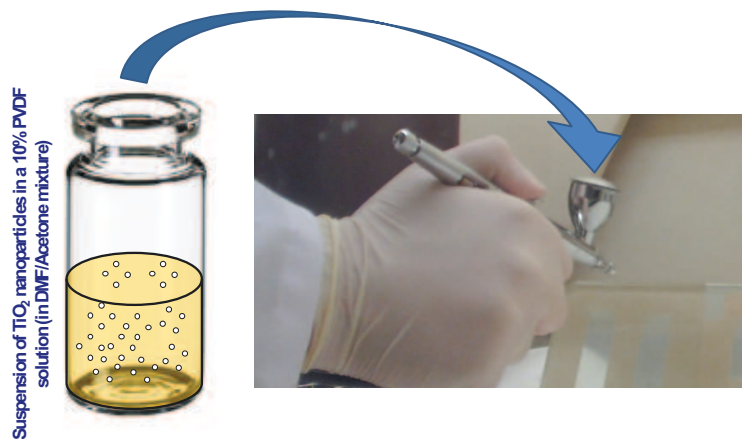


Figure 1

Preparation of TiO₂ suspensions:

- 1 g of PVDF was dissolved in a mixture of 1 mL of DMF and 4 mL of acetone (solution).
- A suspension of TiO₂ in 5 mL of acetone was prepared adding the required amount of nanoparticles as to have a particular composition in the final nanocomposite and sonicating it for 30 min to improve disaggregation of nanoparticles (suspension 1).
- The suspension to be blow-spun (suspension 2) was prepared mixing the solution and suspension 1, stirring for 15 min and sonicating for 15 min in an ultrasound bath at room temperature. Then, the mixture was maintained under agitation until SBS process was carried out. The actual solvent used to prepare the suspensions was then a 10 % v/v solution of DMF in acetone.

The conditions to perform the SBS were the following:

Nozzle diameter: 0.5 mm
 Fluid cup capacity: 5 cm³
 Pressure: 7 bar
 Working distance: 10 cm

Samples in the form of films of about 75 μm were prepared by blow spinning with the airbrush under the above conditions ejecting the material onto a glass plate from which finally they can easily take out (Figure 2).

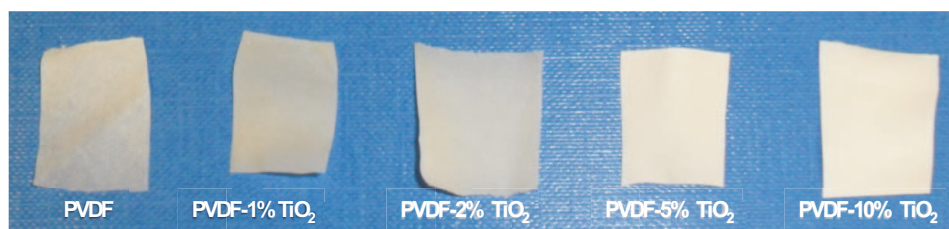


Figure 2

2.3 Characterization methods

Structural studies were carried out by Fourier transformed infrared spectroscopy in middle range, FTIR, and measured with a Nicolet Avatar 360-Golden Gate Diamond FTIR-ATR with temperature controller was used to study the PVDF and the nanocomposites as a function of nanofiller weight percent. Spectra were collected from the average of 64 scans in the range of 4000–600 cm^{-1} , with a resolution of 4 cm^{-1} .

The morphological studies were carried out using a field emission scanning electron microscope Zeiss Ultra 60 (FE-SEM) equipped with a system of X-Ray energy-dispersive spectroscopy (XEDS, with detector Oxford 80 mm^2 X-Max silicon drift) for microanalysis. As the samples were not conductive, they were coated with a very thin layer of carbon using a high resolution ion beam Coater GATAN Model 681 (Extrad Instruments).

The roughness studies were performed by white light interferometry using a NewView™ 7300 3D Optical Surface Profiler (Zygo).

Surface free energy of the different materials was obtained from contact angle measurements. An OCA-15 KRÜSS GmbH tensiometer based on the drop method was used. The contact angle for each testing liquid was obtained from an average using four drops, and the surface free energy was obtained by the Fowkes method [26,27]. As the testing liquids for the contact angle measurements distilled and deionized water, glycerol and diiodomethane were chosen. Table 1 gathers the values of some important parameters of the testing liquids used.

Table 1

Where δ is the density of the liquid, γ_d and γ_p are the dispersive and polar components of the surface tension of the liquids and γ_t the total surface tension or the sum of the polar and dispersive components. The surface tension values were taken from Stöm et al. [28].

The single cell adhesion studies were carried out using an atomic force microscope, AFM, Bioscope II (Veeco Instruments) operated with the Bruker Nanoscope 8.10 software. The AFM is located over an inverted fluorescence microscope Zeiss Axio Observer Z1 equipped with a Hamamatsu C10600 camera with 10 \times and 20 \times objectives, operated with the AxioVision rel. 4.8.2 software of Zeiss. A silicon nitride AFM cantilever without tip, NP-010, supplied by Bruker was used (resonance frequency 12-24 kHz and force constant 0.06 N/m).

2.4 Culture of bacteria

Streptococcus Mutans bacteria, *S. Mutans* (Clarke, ATCC® 25175™), were used for the single cell studies. Its culture was performed in a THB (Todd Hewitt Broth) solution BD Bacto™ TM 249240 (15 g of THB in 500 mL of water). 0.1 μL of the commercial suspension of *S. Mutans* were introduced in a vial with 3 mL of THB solution. Then the suspension was incubated at 37°C, 50% of relative humidity and 2.5% of CO_2 for at least 18 h. After the culture process, the

suspension was diluted 20 times obtaining a concentration of bacteria low enough as to easily visualize them by optical microscopy and subsequently capture one single cell with a home-made AFM tip. Then, the bacteria were stained with two dyes from a LIVE/DEAD® BacLight™ Bacterial Viability Kit (molecular Probes) to monitor bacteria populations as a function of its cellular wall integrity. 0.15 μL of each dye solution were added to the diluted suspension of bacteria.

2.5 Preparation of the AFM tip for bacteria capture

The process followed in this work to prepare the AFM tip and capture bacteria was based in the protocol stated by Beaussart et al. [29]. Basically it can be summarized as follows:

a) Adhesion of a silica bead to the AFM cantilever

With the help of the fluorescence microscope and the AFM, silica beads (4 μm of diameter) were glued to cantilevers using a photocurable adhesive just in the location shown in Figure 3.

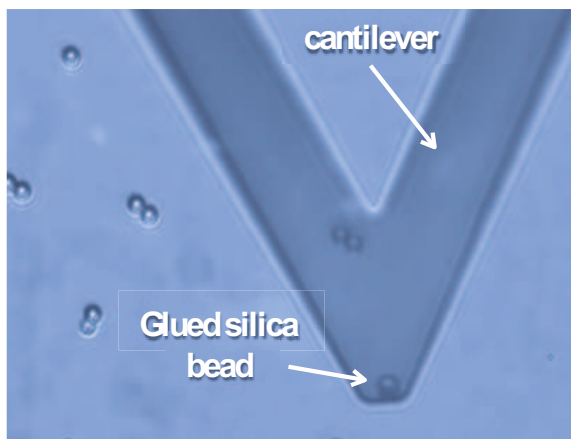


Figure 3

b) Modification of the AFM tip (silica bead)

The fabricated AFM tips were modified with polydopamine, a biological adhesive [30] very appropriate to immobilize bacteria [31].

A 4 $\text{mg}\cdot\text{cm}^{-3}$ dopamine solution at $\text{pH} = 8.5$ was prepared dissolving dopamine hydrochloride 99 % (Aldrich) in a 10 mM buffer solution of Tris-HCl. The cantilever with the glued silica bead was immersed in the dopamine solution for 1h. Then the tip was water washed and nitrogen dried. After that, the force constant of the modified cantilever was determined using the thermal tune mode available in AFM equipment.

c) Bacteria capture

Making use of the optical microscope and the coupled AFM, single bacteria were attached to the ploydopamine modified silica beads (AFM tips). Before making the single cell force spectroscopy measurements, whether the attached stained bacteria were alive or not was tested by fluorescence microscopy.

2.6 Single cell force spectroscopy measurements

The contact between the tip with the attached bacteria and the substrate to be studied was carried out maintaining a maximum load applied of about 1 nN. Then the probe was detached according to the simple mode of obtaining force curves with the AFM. At least 200 force curves were obtained from four different locations on the substrate.

2.7 Data analysis

The software MountainsMap® Universal, version 7.2.7481 (Digital Surf Surface Intelligence) was used to obtain different parameters associated to the roughness from the data obtained with the white light interferometer by mapping the 3D surface, using 5 roughness profiles (Figure 4) and the ISO 4287 standard with a Gaussian filter of 0.08 mm.

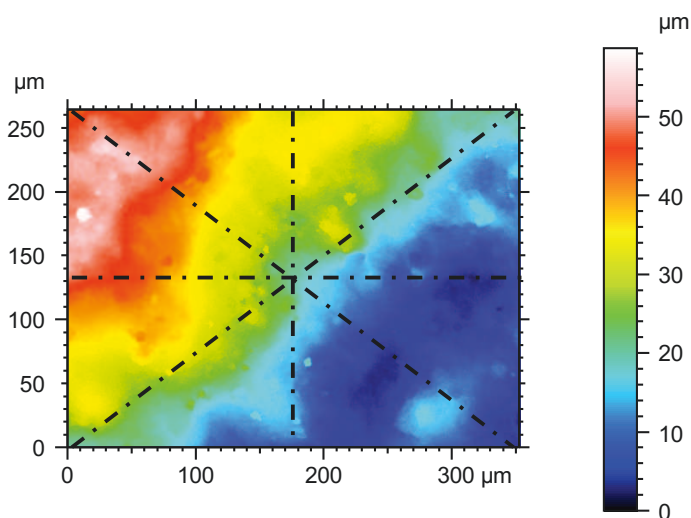


Figure 4.

The parameters thus obtained were:

- Arithmetic mean height, R_a .
- Root mean square height, R_q .

The AFM software was used to convert the original voltage-distance curves to force-distance curves so as to extract the maximum adhesion force and the rupture length for each curve [32]. After that, all the force curves were analyzed to obtain values of adhesion forces and adhesive rupture lengths. A statistical analysis in terms of frequency counting was performed to finally obtain histograms of the adhesion force and adhesive rupture length.

3. Results and discussion

It is well known that PVDF can be prepared with different crystalline phases which can confer different properties to the final material [9]. The most common crystalline phases are α , β , γ and δ . In particular, α -phase arise from the special chains arrangement induced by the trans-gauche conformation (TGTG'). Besides, α -phase has not piezoelectric response since two chains are opposite packed and individual dipole moments are cancelled. In β -phase the chains have all trans conformation (TTTT), resulting in a net dipole moment which yields the highest electroactive properties. γ -phase can be considered intermediate between α and β phases with a gauche bond every fourth repeated units (TTTGTTTG') [33]. Therefore, depending on the proportion between the possible phases of the PVDF different polarities are expected for the surface of the materials. Thus a structural characterization has to be done in order to know if the presence of the TiO₂ nanoparticles can influence in the proportion between the possible crystalline phases of the PVDF and therefore in the final physico-chemical behaviour.

In Figure 5 FTIR spectra of the PVDF with different amounts of TiO₂ nanoparticles are presented. The bands usually assigned to vibrations of the α phase of PVDF (1214, 974, 794, 764 cm⁻¹) [34] are not observed, however, the bands at 1400, 1430, 1274, 1167, 1071, 838 cm⁻¹ assigned to the vibration of the β -PVDF phase and the band 1232 cm⁻¹ assigned to the vibration of γ -PVDF are clearly seen. Besides, as expected it is observed how the broad absorption band at 750-600 cm⁻¹ corresponding to the Ti-O-Ti stretching vibration [35] increases as the amount of TiO₂ increases. On the other hand, it is observed that the IR spectrum of PVDF is practically independent on the TiO₂ nanofiller content. There are not significant bands shifts nor absorbance ratios changes. Thus, it can be concluded that there are not substantial structural variation in the polymer under the influence of TiO₂ nanoparticles mainly showing the presence of the β -phase. As a consequence, none influence is expected in the surface behavior of the materials due to structural changes induced by the presence of the nanoparticles. Here it is also interesting to highlight that SBS under the conditions used in this work is a high efficient method to obtain PVDF with mainly β -phase which is the most wanted phase for future electrical applications due to its piro and piezoelectric properties.

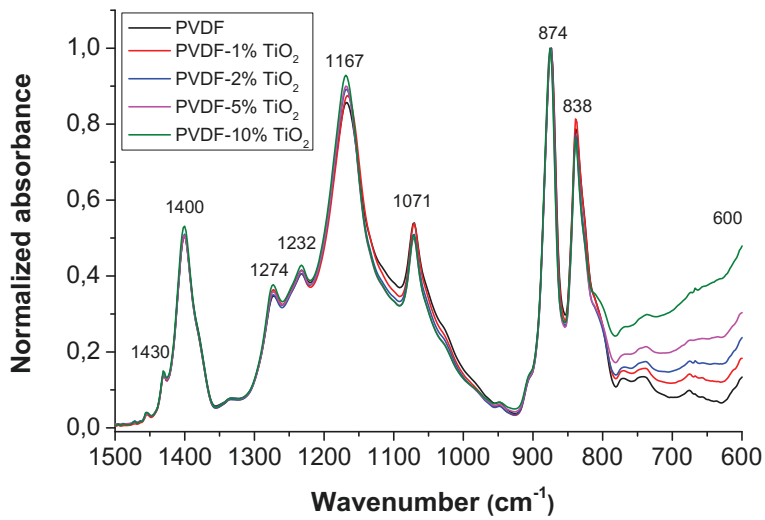


Figure 5.

To study the morphology of the materials at nanoscale SEM images were obtained at different magnifications using the signal coming from secondary, SE, and backscattered, BSE, electrons respectively. Here it is necessary to highlight that topography is highly dependent on the side of the sample film chosen for the analysis. The top side corresponds to the surface directly in contact with air while the bottom is the surface in contact with the glass substrate used to deposit the material during the SBS process. In Figure 6, as an example, the top and bottom surfaces of the same film are shown for a sample of neat PVDF. It can be clearly observed how the bottom surface is much smoother than the top one. The top surface reflects the way the material is deposited on the substrate. Nano- and micro-fibers that, while the blow spinning is taking place, blend each other if solvent evaporation does not completely occur during the material deposition. In fact, the bottom surface simply reflects how the material is spread on the flat glass surface. The rest of composites showed similar topographies when comparing the top surface with the bottom one.

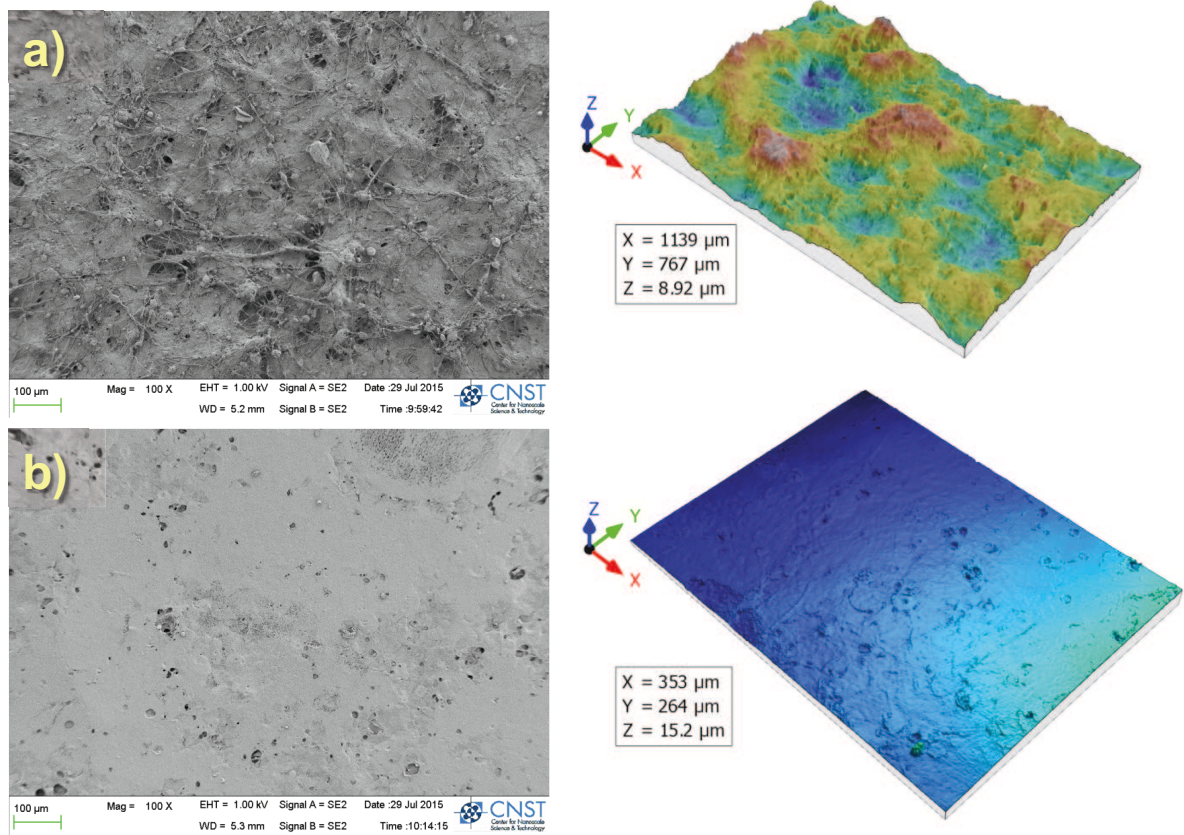


Figure 6.

Certain topographic differences can be observed when comparing the top surfaces of all the materials prepared, what seem to come from the different TiO_2 nanoparticles content (Figure 7). Regardless the composition, the materials show a fiber-like morphology on the surface (diameter of fibers from 100 to 200 nm) which, in general, is due to an arrangement of fibers in the form of bundles (Figure 7f) with a tendency to form like rolled beads interconnected each other (Figure 7). Surprisingly, the higher the amount of TiO_2 nanoparticles the higher the amount of beads (Figure 7), at least up to a concentration of 10 %, for which the number of beads is reduced and the fibers become thinner and better distinguished one another. Sumit Sinha-Ray et al. [36] reported a theoretical and experimental investigation of physical mechanisms responsible for polymer nanofiber formation in solution blowing. However, qualitatively a possible explanation for these results may be associated to the different solvent evaporation rates influenced by the TiO_2 nanoparticles content. If there are competing interactions, for instance, polymer-solvent and polymer-nanoparticles, an increase of polymer-nanoparticles interactions could give more freedom for solvent molecules to favor the evaporation process since it is expected a lower vapor pressure of the solution. A consequence of the later might be a faster increase of viscosity under the presence of TiO_2 nanoparticles when fibers are being created during the SBS favoring the proper fiber formation.

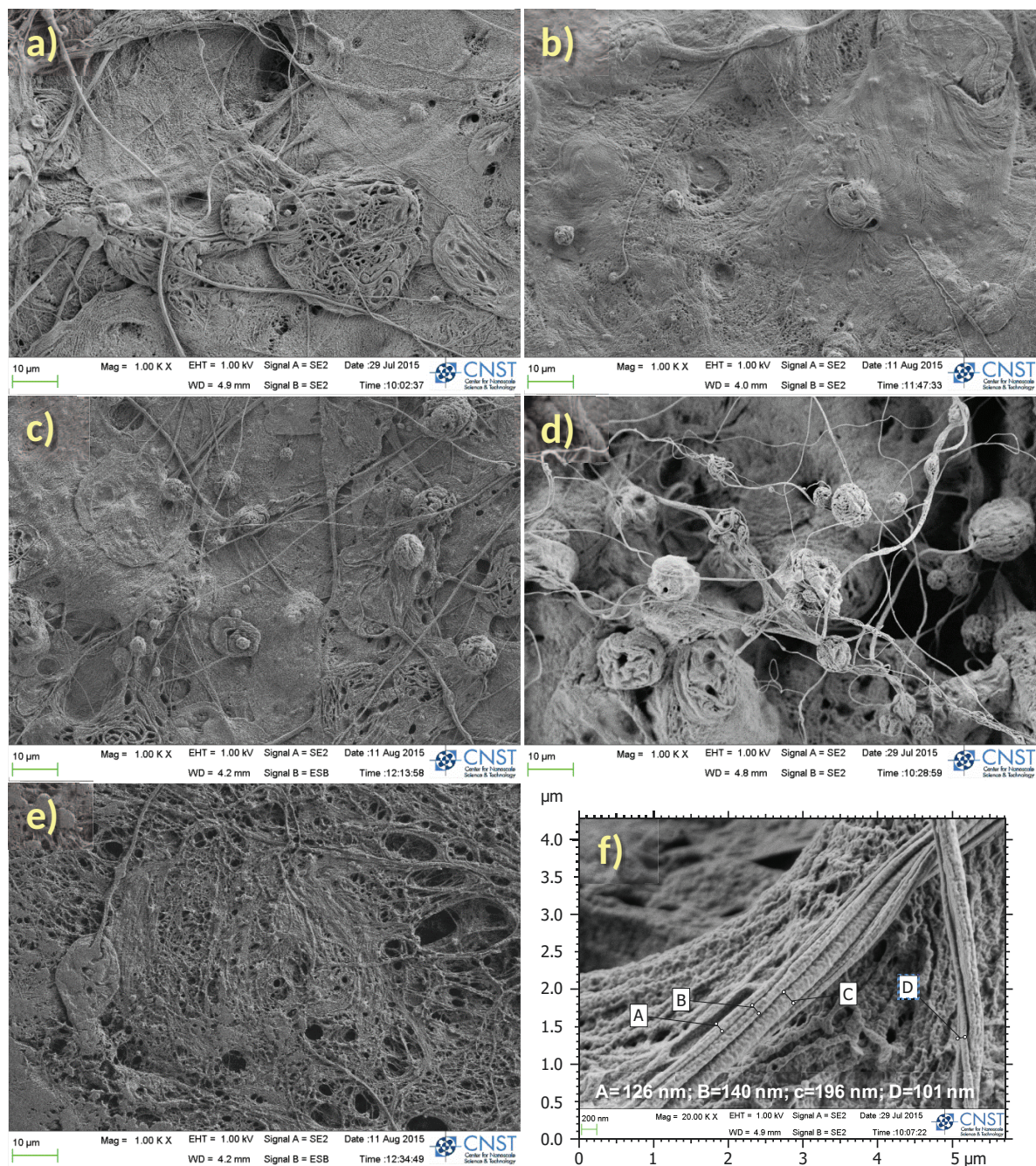


Figure 7.

Another very important point to bring here is the nanofiller dispersion within the polymeric matrix. A uniform dispersion of the nanoparticles is the only way to ensure homogeneity in terms of properties. In Figure 8 (left) it is shown a SEM image obtained from a combination of SE and BSE signals (50 %) of the top surface of a PVDF sample with a 10 % of TiO₂ nanoparticles. Small bright tiny spots (< 100 nm) and small regions (< 400 nm) well dispersed in a dark grey matrix can be observed, and also bright spots located within the fibers all along them (see inset

of Figure 8 left). Those spots and regions can be assigned to the presence of heavier elements which enhance the BSE signal. X-Ray microanalysis on those regions (pointed with an arrow in Figure 8) was performed in order to prove this fact. X-Ray spectra as the one shown in Figure 8 (right) were obtained, evidencing the presence of titanium from the TiO₂ nanoparticles. Therefore, it can be concluded, at least for the system formed by PVDF and TiO₂ nanoparticles, that SBS is a good method to prepare nanocomposites with uniform dispersion of nanoparticles, which get trapped within the polymer when the fibers are formed during the blow spinning process.

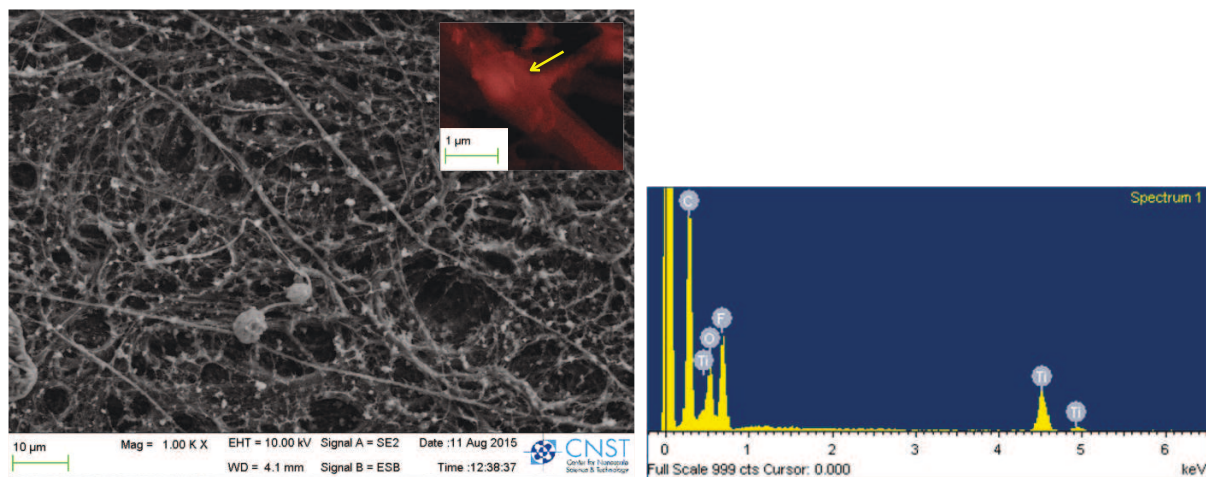


Figure 8.

Apart from the morphology, additional surface characteristics should be studied to interpret cell adhesion data. 3D surface maps were obtained from white light interferometry, from which roughness information can be extracted. In the Table 2 roughness parameters from the average of 5 profiles are gathered for the different materials studied (top sides). Besides, in the case of two samples, pure PVDF and PVDF with 5 % of TiO₂ nanoparticles the analysis was also done for the surfaces corresponding to the bottom side. The inspection of the typical parameters associated to the roughness, R_a and R_q , reflected, accordingly with the observations on SEM images, that there is an initial reduction in the heterogeneity of the topography when a small amount of TiO₂ nanoparticles are added to the PVDF (1 % wt). However, the successive increase of TiO₂ content increases the roughness up to a 10 %, for which a clear reduction in the roughness is again observed. These results confirm what was mentioned above regarding the SEM images.

Table 2

Looking for any correlation with the content of TiO₂ nanoparticles or with the surface characteristics contact angle measurements can also help to interpret the single cell adhesion results to be shown later. The values of contact angle obtained with the three test liquids used are collected in Table 3. Regardless of the test liquid and sample used it is observed that all the contact angles decrease the smoother the side of the samples chosen (bottom side). Therefore

there is an important contribution to the contact angle arising from the roughness of the surface. In particular, the surface is quite more difficult to be wetted, independently of the test liquid, the higher the roughness. The impact of roughness on wettability of a solid substrate is well known [37]. Taking into account that the highest variations in roughness occur for the surfaces corresponding to the top sides of the samples, the discussion in terms of surface free energy should be more easily understood when considering the surfaces of the bottom side.

Table 3

To obtain the surface free energy, γ_s , so as their polar, γ_p , and dispersion, γ_d , contributions the Fowkes method was used [26,27]. The values of surface free energy obtained are gathered in Table 4.

Table 4

The usual value of surface free energy found in the literature for the PVDF is 26 mN/m [38]. As it can be observed for the smoothest surfaces or the bottom sides of the materials, their surface free energy values are similar to the literature values. This result suggests that the unexpected low values of surface free energy for the top side surfaces can be ascribed to the high surface heterogeneity in terms of topography. It is even possible to obtain a very unwettable surface with high roughness values, as it happens in the case of the top side of the PVDF sample with 5 % of TiO₂ that could be considered almost a superhydrophobic surface. Therefore, to examine the samples in terms of the TiO₂ content it is better to compare samples with similar roughness or those corresponding to the bottom side of the materials. In general, it is observed an increase of surface free energy just when a small amount of TiO₂ nanoparticles are within the PVDF (1 %), which comes mainly from an increase of the polar contribution to the surface free energy (Table 4). The value of surface free energy for the bottom part of the PVDF with 5 % TiO₂ confirms the above mentioned since its global value is lower than that of the pure PVDF due to the higher roughness although the polar contribution is higher.

Finally, to study simultaneously direct and indirect (from roughness changes) effects of the presence of TiO₂ nanoparticles on the *S. mutans* adhesion, two samples were chosen: the bottom side of the pure PVDF and PVDF filled with TiO₂ 5 % wt nanoparticles respectively. The election was done considering they show important differences in terms of TiO₂ content but they have small differences in terms of surface free energy. Besides, in both cases the roughness is low enough as to assume absence of adhesion artifacts.

As an example representative force curves obtained for the neat PVDF and PVDF filled with 5 % of TiO₂ are shown in Figure 9. From the deepness and broadness of the minima the values of adhesion forces and rupture lengths were obtained respectively, defining the adhesion force by the difference between the force when the bacteria contacts the surface of the specimen and the force at the peak minimum, while the rupture length is defined by the length measured from the contact point to the rupture point of the last adhesion peak. Regardless the sample and in most of the force curves, two consecutive peaks were always observed, the first one, with strong adhesion values and single sharp ruptures, and the second peak of weaker adhesion at extended rupture lengths. The large adhesion force, also named maximum detachment force, represents the

maximum cell–substrate binding strength at close contact [39]. Detachment of a cell from a solid substrate is a complex process depending on multiple properties like cell geometry, cell elasticity, as well as receptor binding strength, cooperativity and clustering [39]. It seems clear therefore that the *S. mutans* detachment mechanism does not depend on the type of sample inspected but on the intensity of the specific interactions. In fact, comparing between the neat PVDF with PVDF filled with 5 % of TiO₂ nanoparticles the cell adhesion is stronger when the TiO₂ nanoparticles are added to the PVDF by SBS.

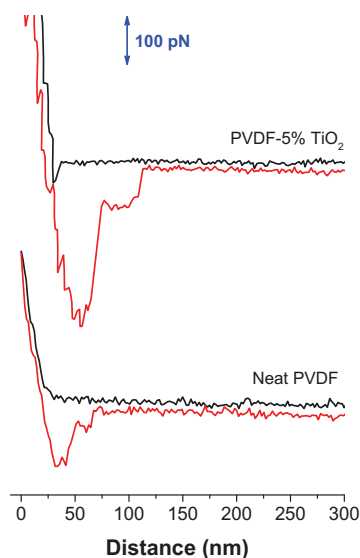


Figure 9.

In Figure 10 the histograms of adhesion forces and ruptures lengths are represented together with the mean values and their standard deviations. Once again, it can be observed how the cell adhesion force with the substrate is lower in the case of neat PVDF. Attending to the surface characterization one would expect stronger adhesion the higher the surface free energy is. In the case of the two samples under consideration (neat PVDF and PVDF with 5 % of TiO₂) it occurs just the opposite. The explanation to these apparently contradictory results may come from the consideration of the roughness and specific interactions between the *S. mutans* cells and the substrates. As can be observed, the slightly lower values of surface free energy for the sample of PVDF with 5 % TiO₂ can be explained from its higher roughness which induced poorer wettability with polar solvents. However, although it has a lower value of global surface free energy, the PVDF with 5 % TiO₂ presents lower contribution of the dispersive part but higher contribution of its polar part, indicating that polar specific interactions should be favored in this case. The latter observation is pointing out therefore that the presence of TiO₂ nanoparticles increases the polar contribution to the surface free energy (Table 4), which must be the cause of the favorable interaction with *S. mutans* cells. This result would be in accordance with microbial adhesion to solvent, MATS, data obtained by E. Preedy et al. for *S. mutans* [40] since this bacteria had quite low affinity for nonpolar solvents at around 8 % for hexadecane and 20 % for decane, suggesting hydrophilic properties. Besides, *S. mutans* had a relatively high affinity for

chloroform (60 %) and low for ethyl acetate, demonstrating its high affinity toward electron acceptor materials [40]. This result is quite relevant when interpreting final antimicrobial behavior of certain nanofillers. In our case, although an antibacterial effect is expected for the TiO₂ nanoparticles, its presence seems to enhance the adhesion of the *S. mutans* which usually is an unwanted phenomenon since it would favor the biofilm development. Although some other works have treated the problem of bacteria adhesion to common polymers, in those cases ideal polymeric surfaces from the chemical and morphological point of view were produced by spin coating the polymer on a silicon substrate [41]. Thus, their results are difficult to extrapolate to those of the present work since the topographical component was avoided.

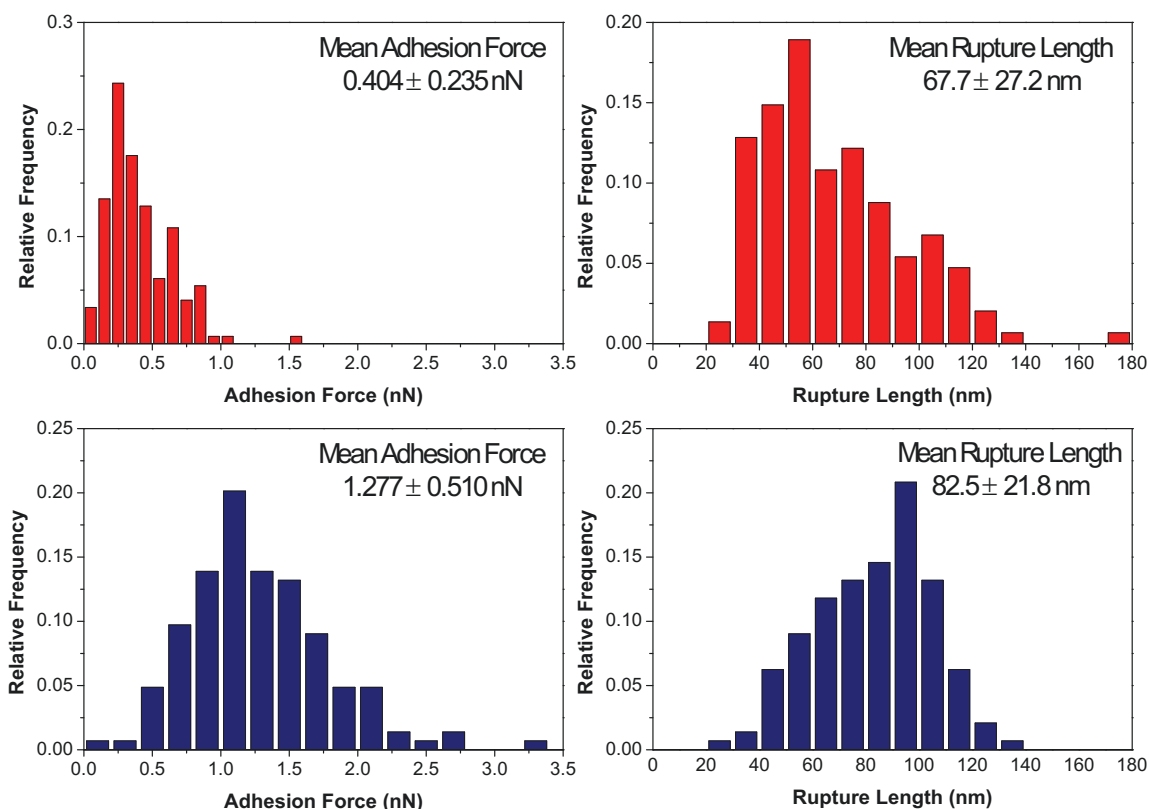


Figure 10.

4. Conclusions

Solution blow spinning is a successful method to prepare films of nanocomposites of TiO₂ based on PVDF showing a fiber-like structure on the surface. Nanoparticles get trapped and quite uniformly dispersed within the polymer when fibers are created during the blow spinning process. The topographies of the films are highly influenced by the TiO₂ content, most likely due to its influence on the solvent evaporation rate. Although the topography greatly conditions the roughness of the samples and as a consequence the surface free energy, actual *S. Mutans*

adhesion on the substrates studied depends mainly on the specific interactions with polar groups. In fact, the presence of TiO₂ nanoparticles increases the polar contribution to the surface free energy, which seems to cause favorable interaction with *S. Mutans* cells.

Acknowledgements

Authors gratefully acknowledge financial support of Ministerio de Economía y competitividad (grant number MAT2014-59116-C2). Furthermore, the authors greatly appreciate The Ministerio de Educación Cultura y Deporte of Spain in the frame of “Modalidad A del Programa de estancias de movilidad de profesores e investigadores en centros extranjeros de enseñanza superior e investigación” for granting the research proposal of Javier González-Benito to do short stay at the National Institute of Standards and Technology, NIST (USA).

5. References

- [1] R.F. Bonan, P.R.F. Bonan, A.U.D. Batista, F.C. Sampaio, A.J.R. Albuquerque, M.C.B. Moraes, et al., In vitro antimicrobial activity of solution blow spun poly (lactic acid)/ polyvinylpyrrolidone nano fi bers loaded with Copaiba (Copaifera sp .) oil, *Mater. Sci. Eng. C*. 48 (2015) 372–377. doi:10.1016/j.msec.2014.12.021.
- [2] A.M. Abdelgawad, S.M. Hudson, O.J. Rojas, Antimicrobial wound dressing nanofiber mats from multicomponent (chitosan/silver-NPs/polyvinyl alcohol) systems, *Carbohydr. Polym.* 100 (2014) 166–178. doi:10.1016/j.carbpol.2012.12.043.
- [3] X. Wang, F. Cheng, J. Gao, L. Wang, Antibacterial wound dressing from chitosan/polyethylene oxide nanofibers mats embedded with silver nanoparticles, *J. Biomater. Appl.* 29 (2014) 1086–1095. doi:10.1177/0885328214554665.
- [4] H.F. Guo, Z.S. Li, S.W. Dong, W.J. Chen, L. Deng, Y.F. Wang, et al., Piezoelectric PU/PVDF electrospun scaffolds for wound healing applications, *Colloids Surfaces B Biointerfaces*. 96 (2012) 29–36. doi:10.1016/j.colsurfb.2012.03.014.
- [5] W. Tutak, S. Sarkar, S. Lin-gibson, T.M. Farooque, G. Jyotsnendu, D. Wang, et al., Biomaterials The support of bone marrow stromal cell differentiation by airbrushed nano fi ber scaffolds, *Biomaterials*. 34 (2013) 2389–2398. doi:10.1016/j.biomaterials.2012.12.020.
- [6] E.N. Bolbasov, Y.G. Anissimov, A. V Pustovoytov, I.A. Khlusov, A.A. Zaitsev, K. V Zaitsev, et al., Ferroelectric polymer scaffolds based on a copolymer of tetra fl uoroethylene with vinylidene fl uoride : Fabrication and properties, *Mater. Sci. Eng. C*. 40 (2014) 32–41. doi:10.1016/j.msec.2014.03.038.
- [7] J. Doshi, D.H. Reneker, Electrospinning process and applications of electrospun fibers, *Conf. Rec. 1993 IEEE Ind. Appl. Conf. Twenty-Eighth IAS Annu. Meet.* 35 (1993) 151–160. doi:10.1109/IAS.1993.299067.
- [8] L.H.C.M. E.S. Medeiros, G.M. Glenn, A.P. Klamczynski, W.J. Orts, Solution blow spinning: a new method to produce micro- and nanofibers from polymer solutions, *J. Appl. Sci.* 113 (2009) 2322–2330. doi:10.1002/app.30275.
- [9] P. Martins, A.C. Lopes, S. Lanceros-Mendez, Electroactive phases of poly(vinylidene fluoride): Determination, processing and applications, *Prog. Polym. Sci.* 39 (2014) 683–

706. doi:10.1016/j.progpolymsci.2013.07.006.
- [10] I. Nieto Pozo, D. Olmos, B. Orgaz, D.K. Božanić, J. González-Benito, Titania nanoparticles prevent development of *Pseudomonas fluorescens* biofilms on polystyrene surfaces, *Mater. Lett.* 127 (2014) 1–3. doi:10.1016/j.matlet.2014.04.073.
- [11] J.M. Arroyo, D. Olmos, B. Orgaz, C.H. Puga, C. San José, J. González-Benito, Effect of the presence of titania nanoparticles in the development of *Pseudomonas fluorescens* biofilms on LDPE, *RSC Adv.* 4 (2014) 51451–51458. doi:10.1039/C4RA09642H.
- [12] W. Bahloul, F. Mélis, V. Bounor-Legaré, P. Cassagnau, Structural characterisation and antibacterial activity of PP/TiO₂ nanocomposites prepared by an in situ sol–gel method, *Mater. Chem. Phys.* 134 (2012) 399–406. doi:10.1016/j.matchemphys.2012.03.008.
- [13] J.M.C. Robertson, P.K. J. Robertson, L.A. Lawton, A comparison of the effectiveness of TiO₂ photocatalysis and UVA photolysis for the destruction of three pathogenic microorganisms, *J. Photochem. Photobiol. A Chem.* 175 (2005) 51–56. doi:10.1016/j.jphotochem.2005.04.033.
- [14] A.G. Rincón, C. Pulgarin, Photocatalytical inactivation of *E. coli*: effect of (continuous–intermittent) light intensity and of (suspended–fixed) TiO₂ concentration, *Appl. Catal. B Environ.* 44 (2003) 263–284. doi:10.1016/S0926-3373(03)00076-6.
- [15] C.C. Trapalis, P. Keivanidis, G. Kordas, M. Zaharescu, M. Crisan, A. Szatvanyi, et al., TiO₂ (Fe₃O₄) nanostructured thin films with antibacterial properties, *Thin Solid Films.* 433 (2003) 186–190. doi:10.1016/S0040-6090(03)00331-6.
- [16] L. Adams, D. Lyon, P. Alvarez, Comparative eco-toxicity of nanoscale TiO₂, SiO₂, and ZnO water suspensions, *Water Res.* 40 (2006) 3527–32. doi:10.1016/j.watres.2006.08.004.
- [17] A.I. Gomes, J.C. Santos, V.J.P. Vilar, R.A.R. Boaventura, Inactivation of Bacteria *E. coli* and photodegradation of humic acids using natural sunlight, *Appl. Catal. B Environ.* 88 (2009) 283–291. doi:10.1016/j.apcatb.2008.11.014.
- [18] R. van Grieken, J. Marugán, C. Pablos, L. Furones, A. López, Comparison between the photocatalytic inactivation of Gram-positive *E. faecalis* and Gram-negative *E. coli* faecal contamination indicator microorganisms, *Appl. Catal. B Environ.* 100 (2010) 212–220. doi:10.1016/j.apcatb.2010.07.034.
- [19] A. Muñoz-Bonilla, A. Kubacka, M. Fernández-García, M. Ferrer, M. Fernández-García, M.L. Cerrada, Visible and ultraviolet antibacterial behavior in PVDF-TiO₂ nanocomposite films, *Eur. Polym. J.* 71 (2015) 412–422. doi:10.1016/j.eurpolymj.2015.08.020.
- [20] N. Hamzah, C.P. Leo, Fouling prevention in the membrane distillation of phenolic-rich solution using superhydrophobic PVDF membrane incorporated with TiO₂ nanoparticles, *Sep. Purif. Technol.* 167 (2016) 79–87. doi:10.1016/j.seppur.2016.05.005.
- [21] K. Prabakaran, S. Mohanty, S.K. Nayak, Influence of surface modified TiO₂ nanoparticles on dielectric properties of PVdF/HFP nanocomposites, *J. Mater. Sci. Mater. Electron.* 25 (2014) 4590–4602. doi:10.1007/s10854-014-2209-3.
- [22] D. Cunliffe, C. a Smart, C. Alexander, E.N. Vulfson, Bacterial Adhesion at Synthetic Surfaces Bacterial Adhesion at Synthetic Surfaces, 65 (1999) 4995–5002.
- [23] B. Cappella, G. Dietler, Force-distance curves by atomic force microscopy, *Surf. Sci. Rep.* 34 (1999) 1–104. doi:10.1016/S0167-5729(99)00003-5.
- [24] M. Benoit, D. Gabriel, G. Gerisch, H.E. Gaub, Discrete interactions in cell adhesion measured by single-molecule force spectroscopy., *Nat. Cell Biol.* 2 (2000) 313–317. doi:10.1038/35014000.

- [25] M. Benoit, H.E. Gaub, Measuring cell adhesion forces with the atomic force microscope at the molecular level, *Cells Tissues Organs*. 172 (2002) 174–189. doi:10.1159/000066964.
- [26] F.M. Fowkes, ATTRACTIVE FORCES AT INTERFACES, *Ind. Eng. Chem.* 56 (1964) 40–52. doi:10.1021/ie50660a008.
- [27] F.M. Fowkes, Donor-Acceptor Interactions at Interfaces, *J. Adhes.* 4 (1972) 155–159. doi:10.1080/00218467208072219.
- [28] B.R. Göran Ström, Monica Fredriksson, Per Stenius, Kinetics of steady-state wetting, *J. Colloid Interface Sci.* 134 (1990) 107–116. doi:10.1016/0021-9797(90)90256-N.
- [29] A. Beaussart, S. El-Kirat-Chatel, R.M.A. Sullan, D. Alsteens, P. Herman, S. Derclaye, et al., Quantifying the forces guiding microbial cell adhesion using single-cell force spectroscopy, *Nat. Protoc.* 9 (2014) 1049–1055. doi:10.1038/nprot.2014.066.
- [30] H. Lee, S.M. Dellatore, W.M. Miller, P.B. Messtersmith, Mussel-Inspired Surface Chemistry for Multifunctional Coatings, *Science*. 318 (2008) 426–430. doi:10.1126/science.1147241.
- [31] S. Kang, M. Elimelech, Bioinspired Single Bacterial Cell Force Spectroscopy, *Langmuir*. 25 (2009) 9656–9659. doi:10.1021/la902247w.
- [32] G. Francius, D. Alsteens, V. Dupres, S. Lebeer, S. De Keersmaecker, J. Vanderleyden, et al., Stretching polysaccharides on live cells using single molecule force spectroscopy., *Nat. Protoc.* 4 (2009) 939–946. doi:10.1038/nprot.2009.65.
- [33] A. Salimi, A.A. Yousefi, FTIR studies of β -phase crystal formation in stretched PVDF films, *Polym. Test.* 22 (2003) 699–704. doi:10.1016/S0142-9418(03)00003-5.
- [34] D. Olmos, F. Montero, G. González-Gaitano, J. González-Benito, Structure and morphology of composites based on polyvinylidene fluoride filled with BaTiO₃ submicrometer particles: Effect of processing and filler content, *Polym. Compos.* 34 (2013) 2094–2104. doi:10.1002/pc.22618.
- [35] L. Liu, H. Chen, F. Yang, Enhancing membrane performance by blending ATRP grafted PMMA-TiO₂ or PMMA-PSBMA-TiO₂ in PVDF, *Sep. Purif. Technol.* 133 (2014) 22–31. doi:10.1016/j.seppur.2014.06.015.
- [36] S. Sinha-Ray, S. Sinha-Ray, A.L. Yarin, B. Pourdeyhimi, Theoretical and experimental investigation of physical mechanisms responsible for polymer nanofiber formation in solution blowing, *Polym. (United Kingdom)*. 56 (2015) 452–462. doi:10.1016/j.polymer.2014.11.019.
- [37] S. Wang, Y. Li, X. Fei, M. Sun, C. Zhang, Y. Li, et al., Preparation of a durable superhydrophobic membrane by electrospinning poly (vinylidene fluoride) (PVDF) mixed with epoxy-siloxane modified SiO₂ nanoparticles: A possible route to superhydrophobic surfaces with low water sliding angle and high water contact, *J. Colloid Interface Sci.* 359 (2011) 380–388. doi:10.1016/j.jcis.2011.04.004.
- [38] W.-K. Lee, C.-S. Ha, Miscibility and surface crystal morphology of blends containing poly(vinylidene fluoride) by atomic force microscopy, *Polymer (Guildf)*. 39 (1998) 7131–7134. doi:10.1016/S0032-3861(97)10081-7.
- [39] J. Helenius, C.-P. Heisenberg, H.E. Gaub, D.J. Muller, Single-cell force spectroscopy, *J. Cell Sci.* 121 (2008) 1785–1791. doi:10.1242/jcs.030999.
- [40] E. Preedy, S. Perni, D. Nipiç, K. Bohinc, P. Prokopovich, Surface Roughness Mediated Adhesion Forces between Borosilicate Glass and Gram Positive Bacteria., *Langmuir*. 30 (2014) 9466–9476. doi:10.1021/la501711t.
- [41] G. Speranza, G. Gottardi, C. Pederzoli, L. Lunelli, R. Canteri, L. Pasquardini, et al., Role

of chemical interactions in bacterial adhesion to polymer surfaces, *Biomaterials*. 25 (2004) 2029–2037. doi:10.1016/j.biomaterials.2003.08.061.

Figure captions

Figure 1. Scheme showing how suspensions of TiO₂ nanoparticles in PVDF solutions are used in the commercial airbrush to blow spun the PVDF based materials on glass substrates.

Figure 2. Films of the PVDF/TiO₂ nanocomposites prepared by SBS with different TiO₂ nanoparticles content.

Figure 3. Position of the silica bead after being glued to the cantilever.

Figure 4. Example of a topographic map obtained from the white light interferometry for the sample PVDF with 1 % of TiO₂. Dashed lines point out the profiles used to calculate the roughness parameters.

Figure 5. FTIR spectra of the PVDF with different amounts of TiO₂ nanoparticles.

Figure 6. Left: SEM (SE signal) representative images of the top (a) and bottom (b) surfaces of blow spun neat PVDF. Right: 3D images traced with MountainsMap® Universal software.

Figure 7. Blow spun nanocomposite materials based on PVDF with different TiO₂ nanoparticles content: a) 0 %; b) 1 %; c) 2 %; d) 5 % and e) 10 % by weight. Image f) shows a detail of a bundle of nanofibers created during the SBS process.

Figure 8. SEM image obtained from a combination of the SE and BSE signals (50 %) of the top surface of a sample of PVDF with a 10 % of TiO₂ nanoparticles (left). X-Ray spectrum obtained in one bright region (marked with the arrow in the SEM image).

Figure 9. Single cell force spectroscopy. Representative force curves (black curve represent bacterial attaching process while red curve represent the bacterial detaching process) obtained for the neat PVDF and PVDF filled with 5 % of TiO₂.

Figure 10. Histograms of adhesion forces and ruptures lengths. PVDF (top) and PVDF filled with 5 % of TiO₂ (bottom).

Tables

Table 1. Values of densities and contributions to the surface tension of the liquids used to carry out the contact angle measurements.

Liquid	δ (g/cm ³)	γ_d (mN/m)	γ_p (mN/m)	γ_t (mN/m)	Supplier
Water	0.998	21.8	51.0	72.8	Home lab
Glycerol	1.259	37.0	26.4	63.4	Panreac
Diiodomethane	3.220	50.8	0.00	50.8	Sigma-Aldrich

Table 2. Roughness parameters from averaging five linear profiles (see Figure 4).

Material	R_q (μm)	R_a (μm)
PVDF-0%	1.90 ± 0.20	1.34 ± 0.22
PVDF-1%	0.51 ± 0.30	0.38 ± 0.25
PVDF-2%	1.43 ± 0.42	0.89 ± 0.31
PVDF-5%	7.00 ± 0.93	4.28 ± 0.70
PVDF-10%	0.37 ± 0.22	0.26 ± 0.18
PVDF-0% (bottom)	0.09 ± 0.01	0.05 ± 0.01
PVDF-5% (bottom)	0.23 ± 0.04	0.17 ± 0.03

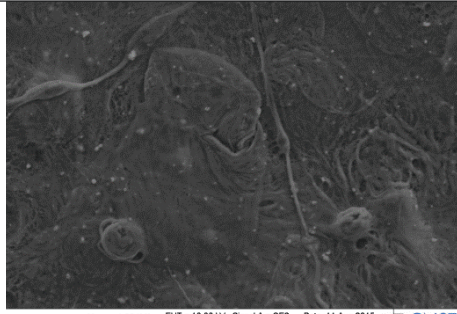
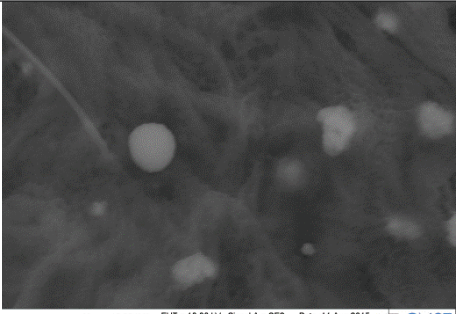
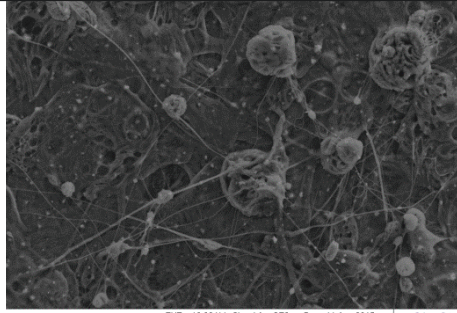
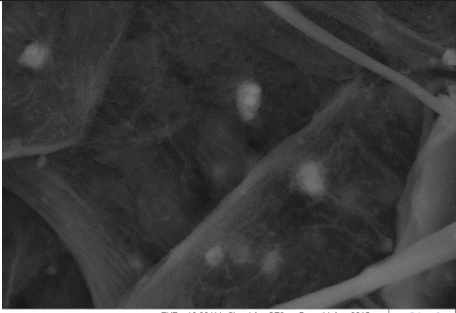
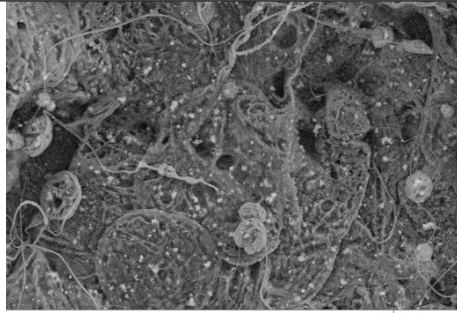
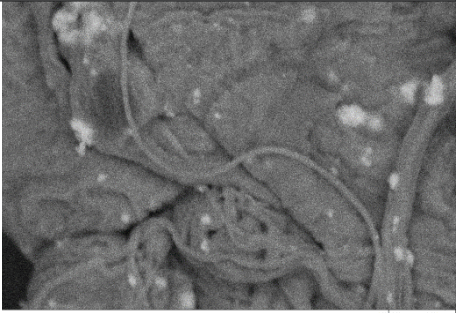
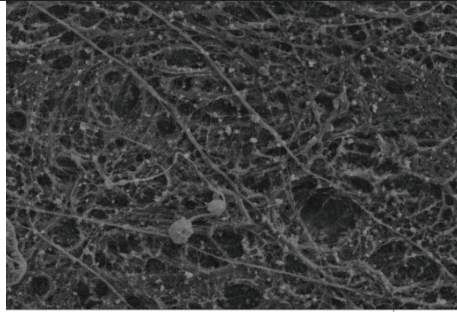
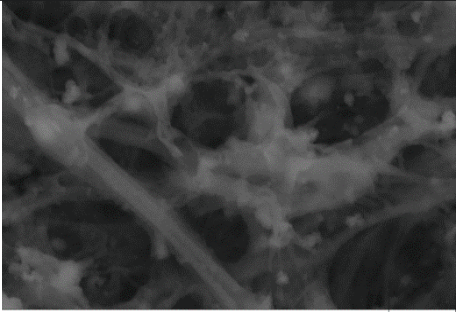
Table 3. Values of contact angle obtained for the different test liquids used.

Sample	Contact Angle ($^\circ$)		
	Water	Glycerol	Diiodomethane
PVDF-0%	120 ± 8	112 ± 9	74 ± 4
PVDF-1%	114 ± 4	104 ± 3	84 ± 4
PVDF-2%	115 ± 6	125 ± 20	83 ± 5
PVDF-5%	143 ± 1	124 ± 2	107 ± 5
PVDF-10%	118 ± 3	105 ± 12	82 ± 2
PVDF-0% (bottom)	102 ± 3	82 ± 3	67 ± 5
PVDF-1% (bottom)	85 ± 2	79 ± 2	71 ± 5
PVDF-2% (bottom)	89 ± 2	84 ± 3	65 ± 4
PVDF-5% (bottom)	103 ± 3	104 ± 4	71 ± 2
PVDF-10% (bottom)	92 ± 3	76 ± 2	66 ± 3

Table 4. Values of surface free energy obtained from the Fowkes Method.

Sample	γ_d (mN/m)	γ_a (mN/m)	γ_p (mN/m)
PVDF-0%	20.7	0.1	20.6
PVDF-1%	15.7	0.3	15.4
PVDF-2%	16.1	0.2	15.9
PVDF-5%	6.7	0.3	6.4
PVDF-10%	16,7	0.0	16.7
PVDF-0% (bottom)	25.3	0.8	24.5
PVDF-1% (bottom)	28.5	6.4	22,1
PVDF-2% (bottom)	29.6	3.8	25,8
PVDF-5% (bottom)	23.0	1.0	22.0
PVDF-10% (bottom)	28.1	3.0	25.1

SEM representative images (taken with backscattered electrons) of samples with different amounts of TiO₂. It can be seen that the higher the amount of TiO₂ the higher number of brighter spots associated to the presence of Ti.

Sample	Magnification	
	1000 ×	10000 ×
PVDF-1%	 <p>10 μm Mag = 1.00 K X EHT = 10.00 kV Signal A = SE2 Date :11 Aug 2015 WD = 4.0 mm Signal B = ESB Time :11:53:52</p>	 <p>1 μm Mag = 10.00 K X EHT = 10.00 kV Signal A = SE2 Date :11 Aug 2015 WD = 3.9 mm Signal B = ESB Time :11:55:00</p>
PVDF-2%	 <p>10 μm Mag = 1.00 K X EHT = 10.00 kV Signal A = SE2 Date :11 Aug 2015 WD = 4.1 mm Signal B = ESB Time :12:23:42</p>	 <p>1 μm Mag = 10.00 K X EHT = 10.00 kV Signal A = SE2 Date :11 Aug 2015 WD = 4.1 mm Signal B = ESB Time :12:25:11</p>
PVDF-5%	 <p>10 μm Mag = 1.00 K X EHT = 10.00 kV Signal A = SE2 Date :29 Jul 2015 WD = 4.7 mm Signal B = SE2 Time :10:43:44</p>	 <p>1 μm Mag = 10.00 K X EHT = 5.00 kV Signal A = ESB Date :29 Jul 2015 WD = 4.7 mm Signal B = SE2 Time :10:36:00</p>
PVDF-10%	 <p>10 μm Mag = 1.00 K X EHT = 10.00 kV Signal A = SE2 Date :11 Aug 2015 WD = 4.1 mm Signal B = ESB Time :12:38:37</p>	 <p>1 μm Mag = 10.00 K X EHT = 10.00 kV Signal A = SE2 Date :11 Aug 2015 WD = 4.1 mm Signal B = ESB Time :12:40:11</p>